SPECTRAL MATCHING WORKING GROUP FINAL REPORT

M. Burgdorf[1], H. Feuchtgruber[2], P. García-Lario[1], T. Müller[1], A. Salama[1]

with the collaboration of:

F. Lahuis[3], S. Lord[4], L. Martin[3], R. Siebenmorgen[1],

SAI/2000-024/Dc, Version 1.2

December 2001

[1] ISO Data Centre, Astrophysics Division, Space Science Department of ESA, Villafranca, P.O. Box 50727, E-28080 Madrid, Spain
[2] Max-Planck-Institut für Extraterrestrische Physik, Postfach 1603, D-85740 Garching, Germany
[3] SRON, P.O. Box 800, NL-9700 AV Groningen, The Netherlands
[4] Centre d'Etude Spatiale des Rayonnements, CNRS-UPS, BP 4346, F-31028 Toulouse, CEDEX 04, France

Document Information

Document:	Spectral Matching WG Final Report
Title:	Spectral Matching WG Final Report
Reference Number:	SAI/2001-024/Dc
Issue:	Version 1.2
Issue Date:	10 December 2001
Editors:	M. Burgdorf & P. Garcia-Lario

Document Change Record

Date	**Revision**	**Comments**
21 November 2000	Version 0.1	First Draft
23 May 2001	Version 0.6	Revised v. with Bibliography added
01 August 2001	Version 1.0	Results updated for pipeline v. 10
20 November 2001	Version 1.1	Revised by P. Garcia-Lario
10 December 2001	Version 1.2	Update by M. Burgdorf

Contents

Chapter 1

Introduction

The Spectral Matching Working Group is one of the eight Calibration Working Groups constituted at the ISO Data Centre to address different calibration topics during the Post-Operational Phase of the ISO Project in the framework of the global ISO (Cross-)Calibration strategy.

The Working Group scheme was invented as a platform to exchange knowledge and progress between the members of each of these Working Groups, across instrument boundaries and major themes of common interest.

1.1 Purpose of the Spectral Matching WG

The purpose of the Spectral Matching WG, as stated in the ISO (Cross-)Calibration Plan for Post-Operations, is to:

- Characterization of the Relative Spectral Response Function (RSRF) for all ISO spectroscopic observations.
- Analysis of spectral matching between LWS and SWS in the overlapping region. Same with CAM-CVF, PHT-S and SWS spectra. Comparison with astronomical models.
- Identification of possible systematic errors in the measured spectral response to extended sources by comparing the observations from a variety of instruments. Effects on the determination of spectral line fluxes.
- Expansion of cross-calibration between the instruments beyond the wavelength regions which they have in common.

1.2 Spectral Matching WG Webpage

The Spectral Matching WG WWW page is maintained by M. Burgdorf at:

`http://isowww.vilspa.esa.es:1909/~mburgdor/.`

This page contains information on the latest meetings held by the Working Group, including in most cases the viewgraphs there presented (internal access only).

Chapter 2

Comparison of SWS and LWS Spectra in Overlap Region

The Spectral Matching Working Group was originally created as an attempt to investigate discontinuities between SWS and LWS in complete ISO spectra from 2 through 200 μm. In order to determine the extent of the problem, a software tool was developed which automatically selected observations made with SWS and LWS on the same coordinates and which calculated the ratio of the fluxes in the overlap region from the browser products. This way all observations with the spectrometers could be checked for possible discrepancies, provided that they were performed with standard Astronomical Observing Templates and covered the wavelength range that SWS and LWS have in common. The program that was used for this purpose was only intended for use by the Working Groups; its functionality can be fulfilled, however, by User Defined Functions as well. All results described in this chapter are based on the analysis of pipeline products.

2.1 Summary of Results

A total number of 122 common pointings were selected from the ISO Data Archive for which both SWS and LWS measurements of bright sources (fluxes higher than 100 Jy at the overlapping region) were available.

In order to estimate the level of agreement between both instruments, we used ISAP v2.1 to derived the average value of the flux in the overlapping spectral range between 43.7 and 44.4 μm of each of the OLP v10 SWS and LWS spectra included in our cross-calibration sample. This way we estimated the LWS/SWS ratios at 44 μm for each of the 122 different pointings above mentioned obtaining that only 50% of them showed a flux ratio LWS/SWS at this wavelength within 20% from unity.

The discrepant sources in the sample showed ratios in the range 0.7 to 12 (see Fig. 1). In order to investigate more in detail the reasons for the wide distribution of values observed, a detailed analysis of the nature of the sources in the sample showing discrepant values (consistency worse than 20%) was carried out.

Ratios between 1.2 and 6 can naturally be explained if they correspond to extended sources. This is because the aperture increases from $20'' \times 38''$ for band 4 in SWS to $71''$ (a factor of 6.1 larger) for band SW1 in LWS. Thus, stronger LWS fluxes are expected from extended sources.

This was the case of most of the H II regions included in the sample. They showed ratios in the above range and were identified as extended sources in the literature.

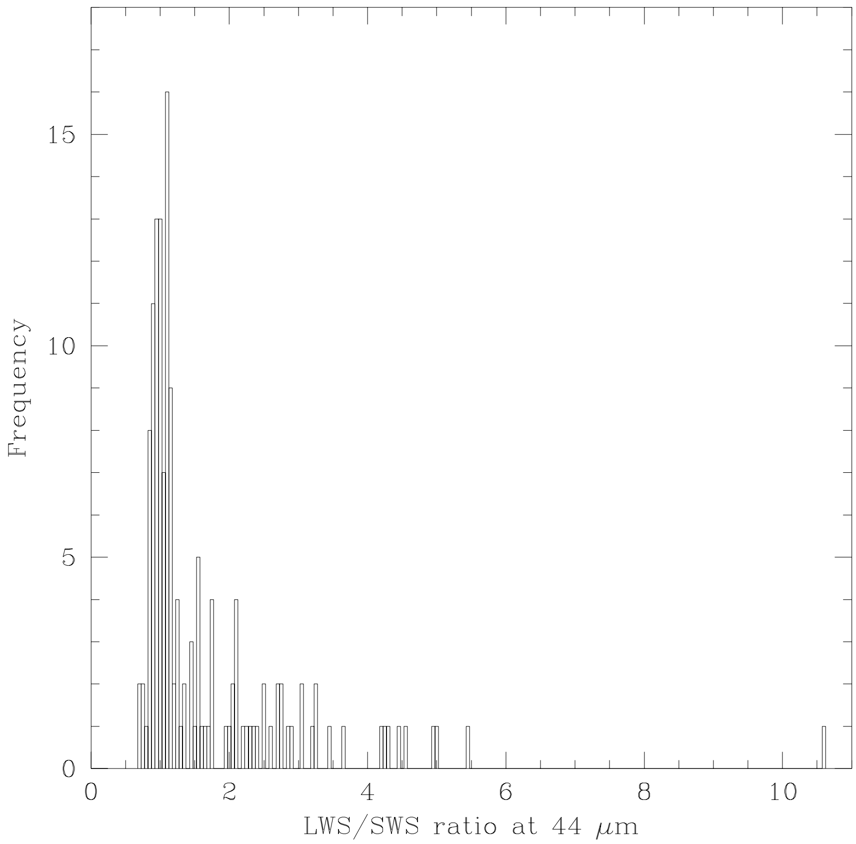

Figure 2.1: *Distribution of LWS/SWS ratios at 44 μm for all sources in the original sample*

In all cases, their extended nature was confirmed through the detection of similar discontinuities between the SWS bands 3D and 3E at 27.5 μm and 3E and 4 at 29 μm where the aperture changes from a size of $14'' \times 27''$ (band 3D) to $20'' \times 27''$ (band 3E) and to $20'' \times 33''$ (band 4).

Sometimes also jumps are observed betwen bands 2C and 3A at 12 μm where there is also a change in the aperture size. Other extended sources were also identified this way and removed from the sample.

The only object showing a value of the LWS/SWS ratio larger than 6 was found to correspond to a bad-pointed SWS observation of an extended object leading to a strong underestimation of the SWS flux at 44 μm.

A few other bad pointed observations were also identified by the strong band mismatches (inconsistent with an extended nature) found in their SWS spectra and were also discarded.

Finally, in order to avoid also dealing with objects showing a strong photometric variability, sources classified in the literature as pulsating AGB stars (like all the variable Mira and OH/IR stars) in the cross-calibration sample were also identified and removed from the analysis, with the only exception of those sources observed with LWS and SWS on the same revolution (usually one after the other), since in this case their intrinsic variability does not affect our cross-calibration analysis.

When all the objects recognized as variable and extended sources are removed from the cross-calibration sample and ignoring also all the suspected bad-pointed observations, we end up with a short list of about 25 good test cases for which we show the LWS/SWS ratios at 44 μm derived using ISAP v2.1 in Table 3.1.

Table 2.1: *OLP v10 LWS/SWS ratios at 44 μm sorted by LWS TDT number*

Source	SWS TDT#	LWS TDT#	LWS/SWS	SW1/SW2	Notes
HD 161796	07100579	07100579	0.75	0.80	
HD 101584	07901402	07901520	0.81	0.78	
Hen 2−113	07903307	07903229	0.78	0.81	
HD 161796	07100579	08001732	0.83	0.78	
CPD −56 8032	27301339	08401538	0.83	0.80	
IRAS 16342−3814	45801328	08402827	0.74	0.78	
Circinus	07902231	10401133	1.06	0.70	bad SWS band 4
AFGL 4106	10401225	10401227	0.75	0.85	
M 1−78	15901853	15901854	0.70	0.73	
CW Leo	19700159	19800158	0.91	0.82	
μ Cep	08001274	22002005	0.87	–	strong near-ir leaks
SAO 34504	2630215	26300513	1.12	1.07	bad SWS band 4
IRAS 19114+0002	52000234	31900901	0.96	1.03	
OH 26.5+0.6	33000525	33000316	1.01	1.04	
VX Sgr	09900171	33100802	1.04	1.03	
IRAS 15452−5459	45900615	48800916	1.12	0.96	slightly extended?
IRAS 16594−4656	45800441	49001642	1.02	1.01	
IRAS 19114+0002	52000234	52500861	1.00	1.03	
R Dor	58900918	59300644	1.03	–	strong near-IR leaks
Hen 2−113	07903307	60701891	1.07	1.06	
CRL 618	68800561	6880450	0.90	1.08	bad SWS band 4
IC 418	82901301	68900805	1.04	1.14	
TX Cam	69501070	69501069	1.06	1.03	
HD 44179	70201801	70201904	1.00	1.06	
IC 418	82901301	86801205	1.03	1.00	

As we can see there is a strong difference in the behaviour of the LWS/SWS ratios observed before revolution 220 and after revolution 263. If we exclude from the analysis the few objects showing calibration problems in band 4 of SWS (usually strong mismatches with band 3) which are indicated in Table 3.1 we see that the mean LWS/SWS ratio before revolution 220 is <LWS/SWS> = 0.78, with very little dispersion around this value (r.m.s = 0.05) suggesting a systematic underestimation ($\sim$ 22%) of the flux recorded in the SW1 detector of LWS with respect to SWS band 4. However, taking all the values not affected by any problem in SWS band 4 after revolution 263 we see that the mean value now obtained is <LWS/SWS> = 1.02, very close to unity, and also with a very low dispersion, with all the ratios being within 10% of this mean value. This is remarkable, if we consider that LWS and SWS were calibrated in a totally different way (LWS calibration is based on Uranus as primary calibrator while SWS band 4 calibration is mainly based on ground-based ILT experiments using blackbody sources).

Looking for the reason of the systematic mismatch between SWS and LWS in the first 200 revolutions of ISO we also searched for the quality of the spectral matching between detectors SW1 and SW2 of LWS. Looking again at Table 3.1, where we have also plotted the SW1/SW2 ratios derived from ISAP v2.1 at the overlapping wavelength, it is clear that the peculiar behaviour observed in the SW1 detector of LWS is not followed by SW2, which is in almost perfet agreement with SW1 only after revolution 263 and shows the same kind of discrepancy with SW1 as band 4 of SWS before revolution 220.

Moreover, one of the objects in our list of cross-calibration sources, the planetary nebula Hen 2−113 was observed at two different epochs with LWS, one in revolution 79 (before revolution 222) and another one in revolution 607 (after revolution 263). As we can see in Table 3.1 the behaviour of SW1 is completely different for the same source depending on the revolution

Detectors	Ratio of Fluxes
SW1/SW2	0.95598
SW2/SW3	1.00971
SW3/SW4	1.00492
SW4/SW5	1.00798
SW5/LW1	1.04758
LW1/LW2	1.07360
LW2/LW3	1.04000
LW3/LW4	0.985711
LW4/LW5	0.901091

Table 2.2: Fluxes from Overlapping Detectors.

considered and it follows the general trend described above.

From this analysis we concluded that there must be a calibration problem affecting only detector SW1 of LWS from the early days of ISO and until a moment in the mission somewhere between revolutions 220 and 263. Looking into possible explanations we found that the bad flux calibration of SW1 might be related with a change in the illuminator flash sequence introduced in revolution 236 and with how this is processed in OLP v10.

In order to check for this possibility, we searched in the ISO Data Archive all the previous observations taken with LWS before and after this revolution 236 and we can confirm that the strong change in the calibrated SW1 flux takes place exactly on this revolution. Further investigation is now required to correct this problem, which at first sight only affects detector SW1.

All the cross-calibration test cases used in the confection of Table 3.1 are shown in Figs. 2 to 5, where the anomalous behaviour of SW1 is clear in all the spectra taken before revolution 236 (Figs. 2 and 3) while we show also how there is an almost perfect agreement between SWS and LWS for the sources observed after this revolution (Figs. 4 and 5).

As a byproduct of this analysis and since in several cases objects were repeatedly observed throughout the mission with either SWS or LWS, it was also possible to perform an independent analysis of the stability of both instruments, SWS and LWS in terms of absolute flux calibration. The results obtained indicate that for both LWS and SWS the reproducibility is better than 15% in all cases, although for SWS the number of suitable observations is relatively small (see Figs. 6 and 7).

2.2 Problems

2.2.1 Stitching between SW1 and SW2

The ratio between neighbouring detectors for all L01 observations was calculated from the browser products. The following table gives the result (rejecting a few obvious outliers where the overlapping detectors differ by more than a factor of 2):

The following is worth mentioning:

- Detectors SW2 - SW5 stitch already in the browser product better than 1 %, therefore it appears that they define the absolute flux level in a more reliable way than SW1

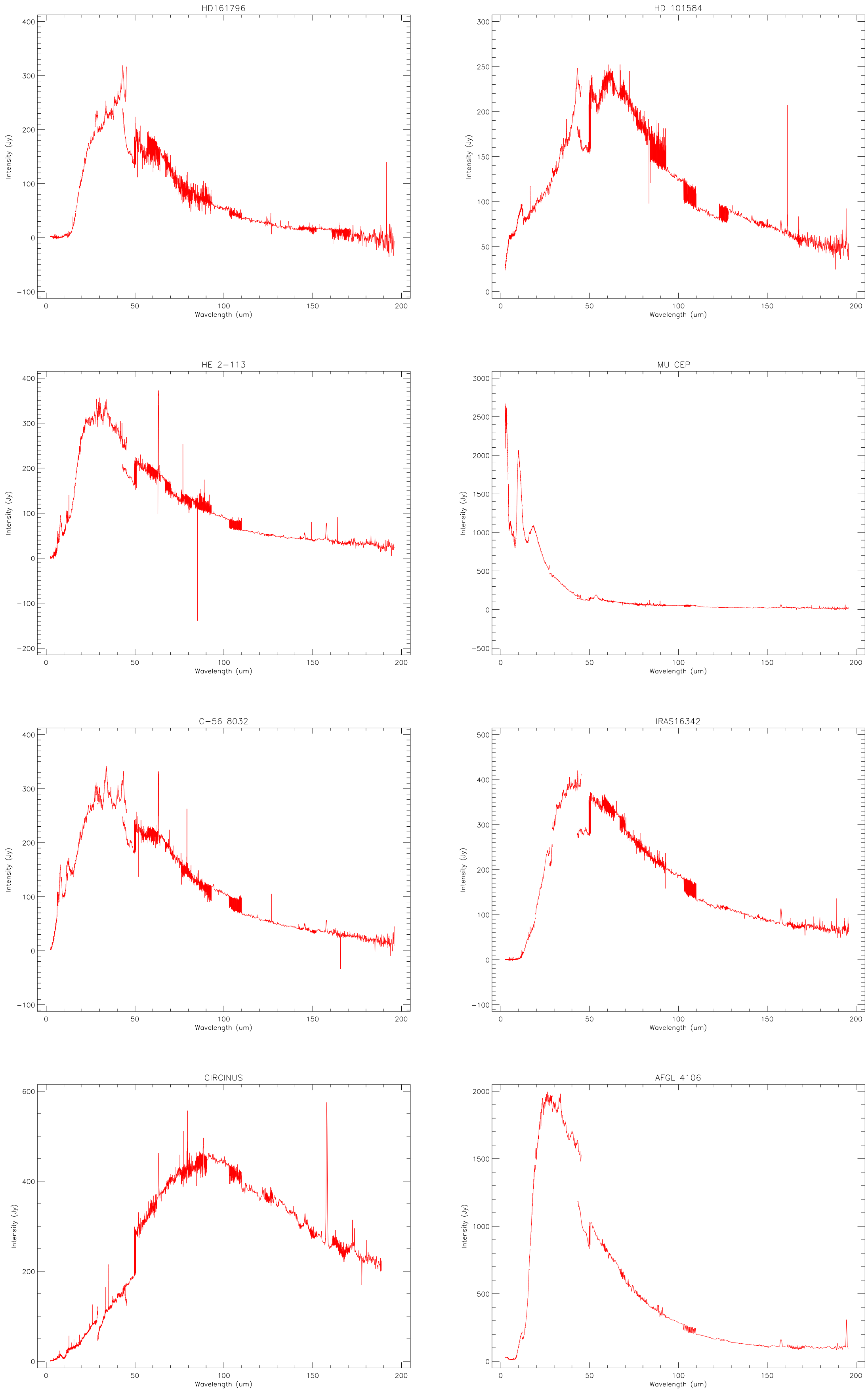

Figure 2.2: *Composite OLP v10 SWS+LWS spectra of sources observed before revolution 236. Note the 20% mismatching of SW1 with the adjacent detectors.*

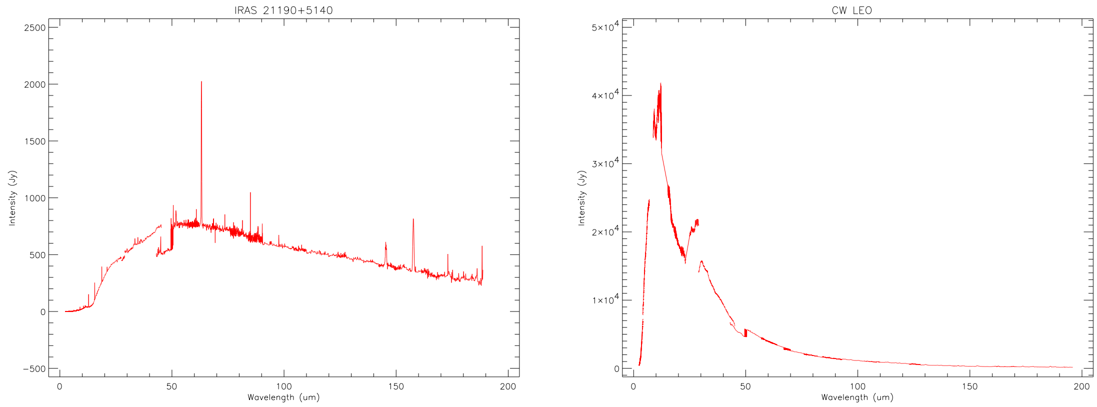

Figure 2.3: *Additional composite OLP v10 SWS+LWS spectra of sources observed after revolution 236. Note in this case the perfect matching of SW1 with the adjacent detectors.*

- Only two ratios are off by more than 5 %
- Detector LW5 seems to lie too high, since calculating LW4/LW5 for nine different sets of 100 revolutions gave in each set a value significantly lower than 1. This is the case even though one would expect the opposite effect from extended sources which are included in the samples
- No obvious trends with time were found in the quality of the stitching

2.2.2 Memory Effects in Ge:Be

- SWS

  The amplitude of the transient effects are typically of the order of 10-20 % of the flux step (assuming a some-what constant flux before and after the step) with a decay-time of order 100 seconds.

  The effect of the transients is two-fold:

  - transient affecting the dark currents
  - transient after flux steps (e.g. in up-scan after dark current)

  Figure 5 shows the magnitude of the transient.
  These data are based on a study on a full sample of AOT-1 observations to make a first inventory of SWS transients and to help in further developing and testing correction models.

- LWS

  Due to the scanning sequence of LWS it is assumed that transient effects there can almost be neglected. It is assumed that the effects for LWS SW1 will be similar than for SWS. However with an LWS full scans from very low responsivity to full and back are made. This sort of makes sure that the detectors are most of the time in a settled state since hardly any signal 'jumps' are made (except for the case of strong lines) like with an SWS AOT-1 scan. Even though there are differences in the measured signals from forward and backward scans for certain detectors (e. g. LW2), they are relatively small.

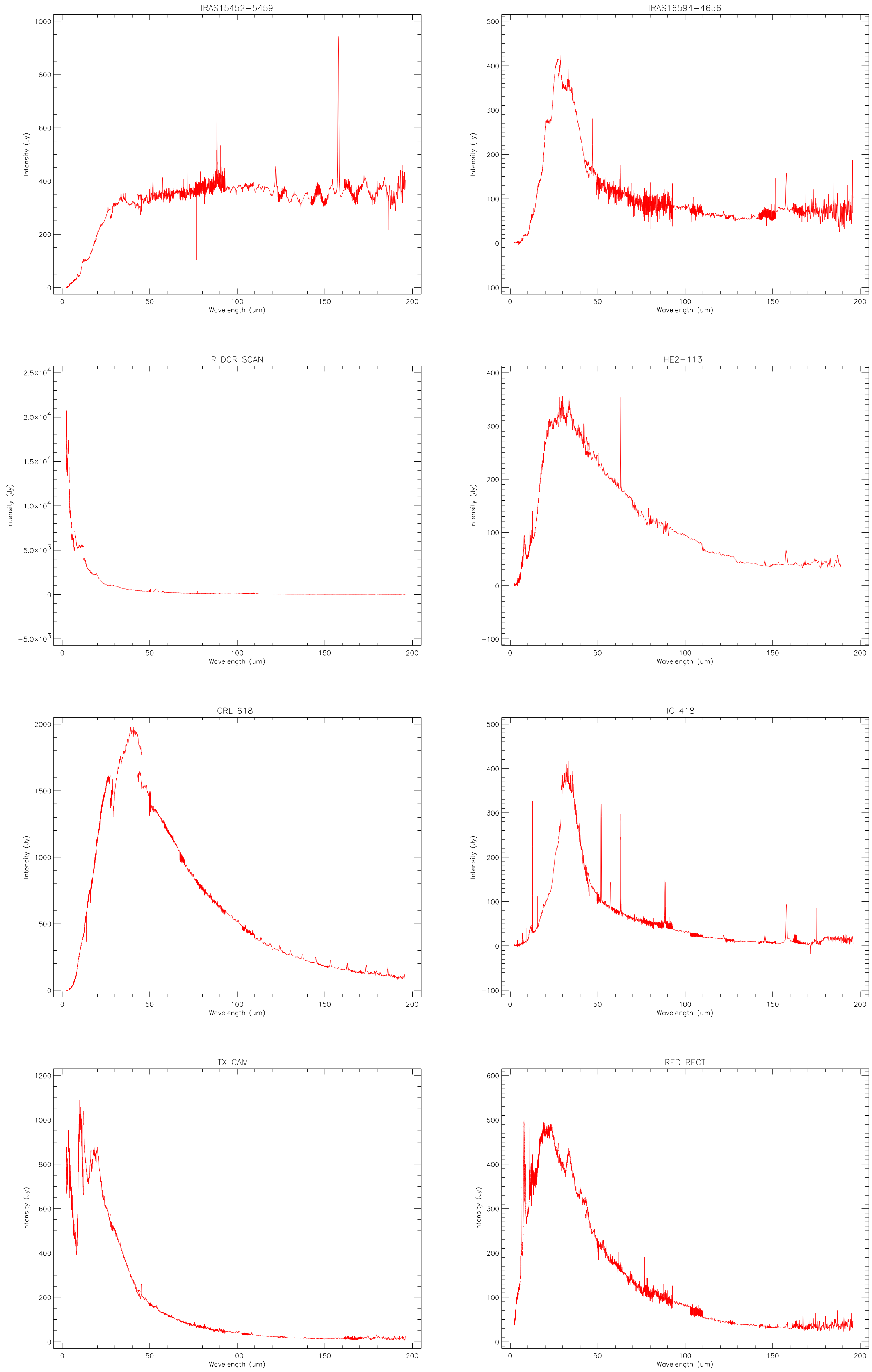

Figure 2.4: *Additional composite OLP v10 SWS+LWS spectra of sources observed after revolution 236. Note in this case the perfect matching of SW1 with the adjacent detectors.*

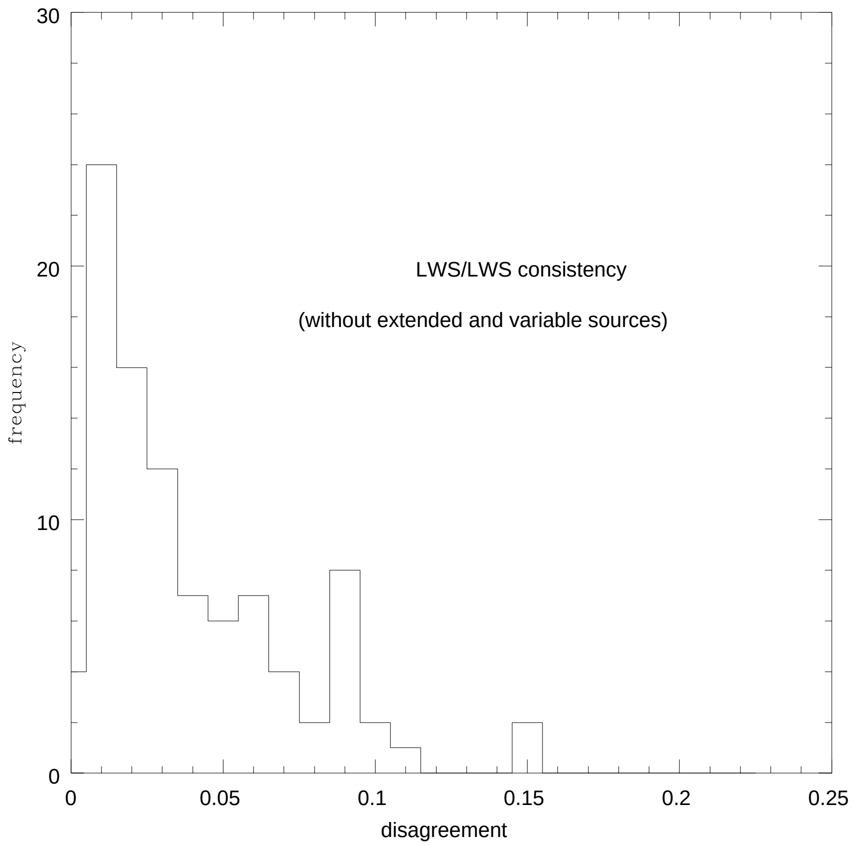

Figure 2.5: *Flux reproducibility with the LWS*

- Example

  The spectrum of VY CMa e.g. is clearly affected by transient effects. This however has only a small impact. See the plots in figure 6.

  In the case of VY CMa the amplitude of the error in the standard dark current calculation will be of order 50-100 μV/s and the transient tail in the up scan will be app. 300 Jy (100 μV/s / 0.3 (RSRF @ 45 μm)).

  If these effects are disregarded and the up and down scan are simply averaged a total error in the AAR at the long wavelength part of app. 300-400 Jy can easily be made and an error at the key wavelength of a 100 Jy.

  In this case (as has been shown by H. Feuchtgruber) other effects are clearly playing a role. At these high fluxes there appears to be a change in the response of the detectors with changing flux????

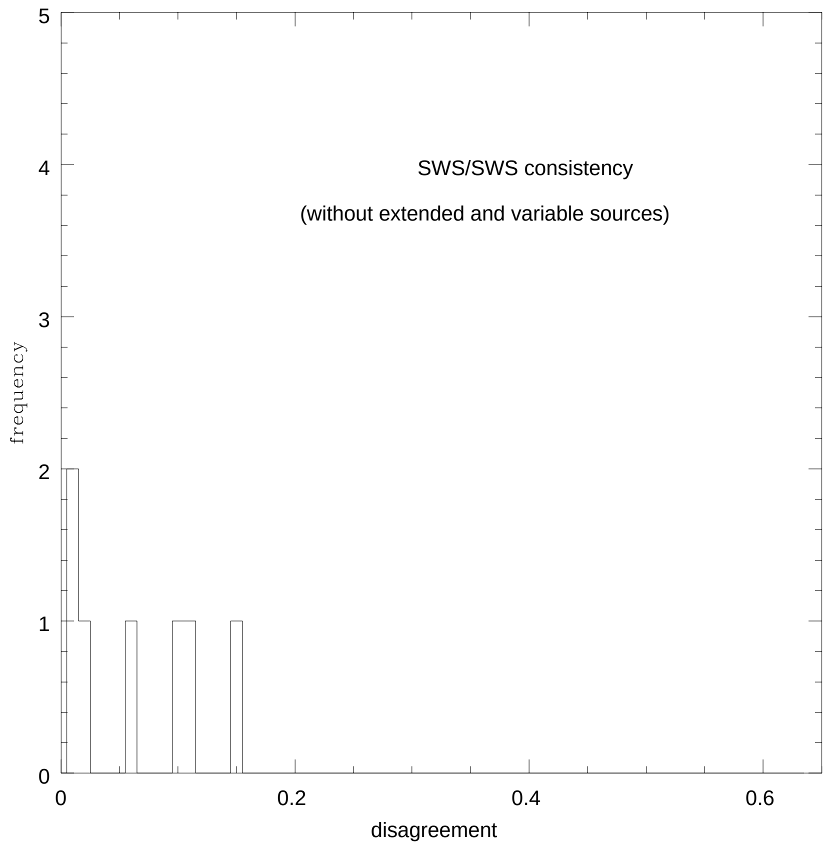

Figure 2.6: *Flux reproducibility with the SWS*

2.3 Extended Sources

As the instruments aboard ISO have different apertures, it is very difficult to match their spectra of extended sources. An interesting case is NGC4945, where the fluxes measured by LWS and SWS at 45 μm differ by more than a factor of four (see figures 7 and 8). This result is difficult to explain only by the difference of apertures, because all of the far-infrared luminosity was claimed to originate from a nuclear source no larger than 12" $\times$ 9" in extent (Brock *et al.* 1988). This is much smaller than the apertures of both SWS (20" $\times$ 33") and LWS (38" radius). An error in the absolute photometry for extended sources of this size, however, can be ruled out from comparisons made for each instrument separately with IRAS (see Brauher & Lord 2001 and chapters 3.4.2 and 3.4.4 of the 4th Post-Operations Cross-Calibration Status Report,

`http://www.iso.vilspa.esa.es/users/expl_lib/performance.html`

). We have to conclude therefore that the size of the central source at wavelength 45 μm is larger than 30" (see also Ghosh *et al.* 1992).

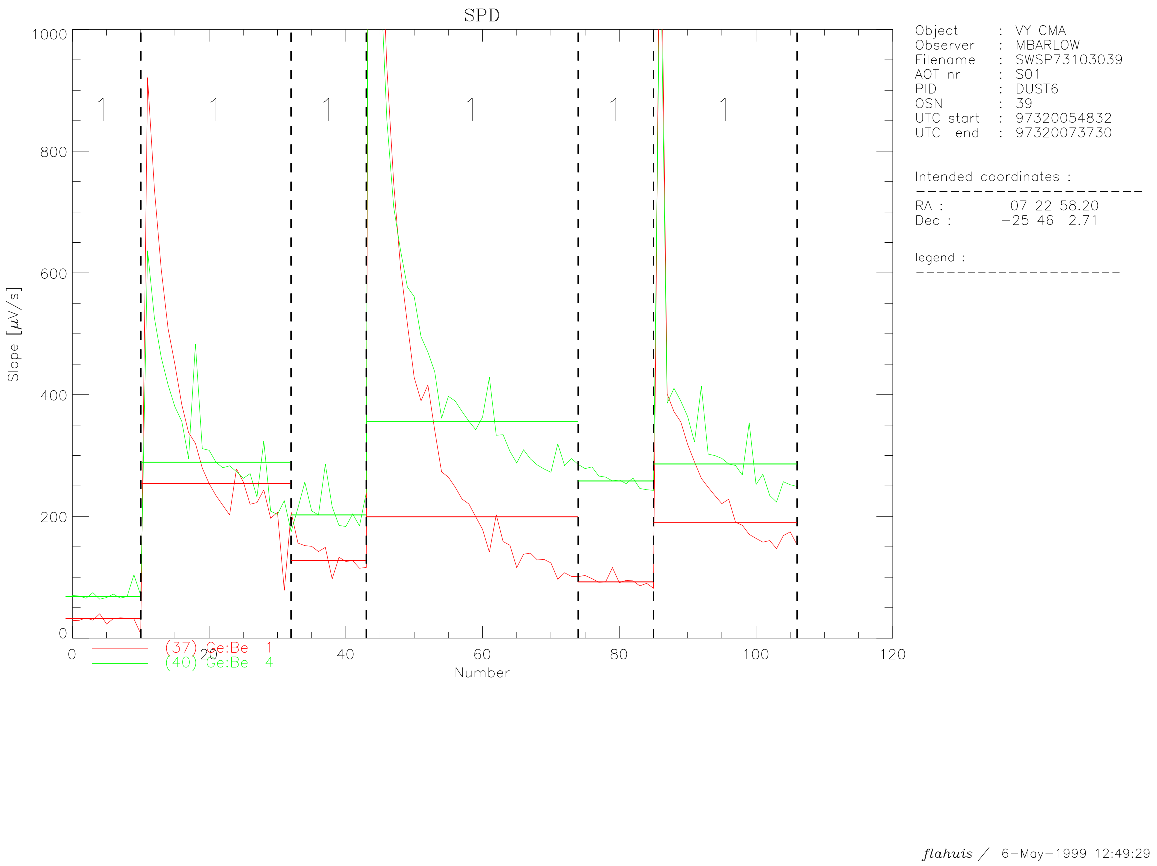

Figure 2.7: *Difference of signal in scans from the same observation with SWS*

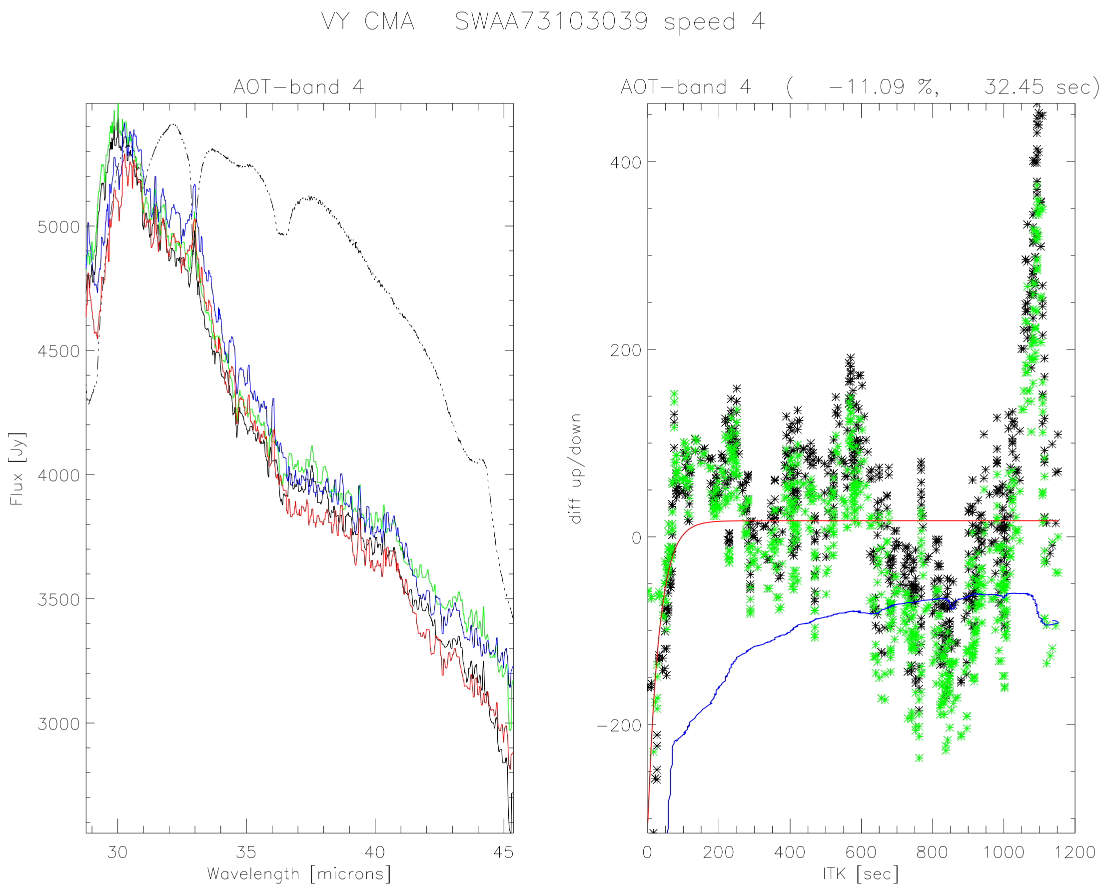

Figure 2.8: *The flux from VY CMa in up and down scans as measured with SWS*

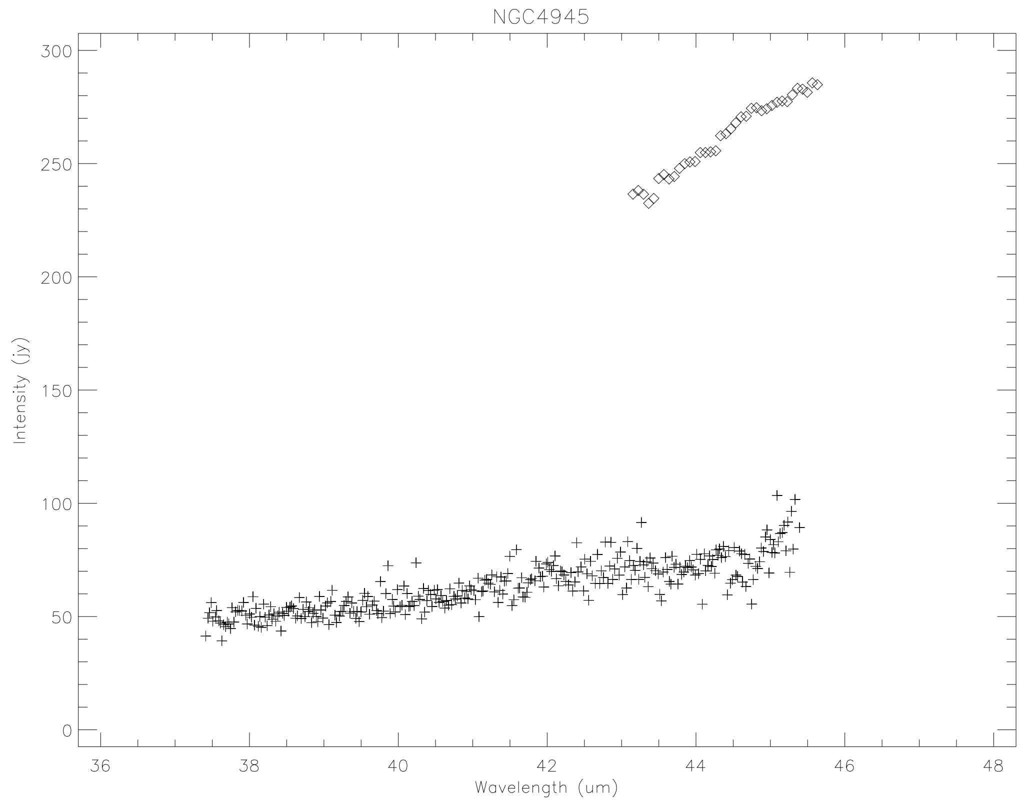

Figure 2.9: *The flux from NGC 4945 as measured with SWS (plus signs) and LWS (diamonds)*

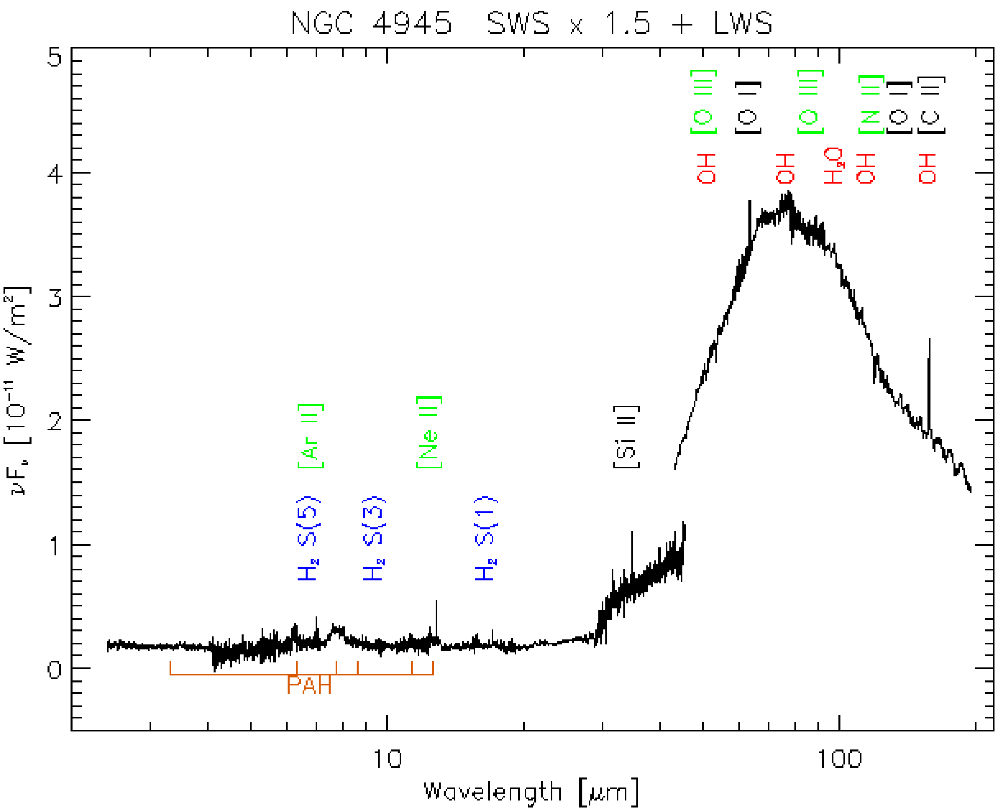

Figure 2.10: *The complete spectrum from NGC 4945 after correction for the different apertures of the spectrometers*

Chapter 3

Comparison of Lines in Spectra from Different Instruments

In the previous chapter we showed that the flux calibration of the two spectrometers aboard ISO agrees in a satisfactory way for continuum sources. In this chapter we investigate the question whether this is also the case for spectral lines. As scanning over a spectral line exposes the photoconductive detectors to a quickly varying illumination, transient responses might affect the measured line strengths. We present therefore in the following not only comparisons between ISO's spectrometers but also between ISO and KAO line fluxes in order to provide an independent check. These and the following chapters show results obtained from products of pipeline version 8 that were further processed with LIA (LWS Interactive Analysis Software, Sidher *et al.* 1997).

3.1 Comparison of Lines from the same Molecule in SWS and LWS

3.1.1 Water Lines on Mars

Even though water is only a minor constituent of the Martian atmosphere (its mixing ratio is 3×10^{-4} at the surface), its lines dominate the spectra taken with SWS and LWS of this planet. As the flux in the line center is known from models, one can use its ratio to the continuum in order to determine the mean disk emissivity at the wavelength of the lines. Hence one can obtain from the analysis of all the water lines a sparsely sampled spectrum of the continuum flux that only relies on the measured strengths of the lines (for details of this method see Burgdorf *et al.* 2000). Figures 9 and 10 show the result for SWS and LWS, respectively.

Near 45 μm SWS gives an emissivity of 0.90 whereas one finds from LWS data values closer to 0.98. Unfortunately the lines in the overlap region between SWS and LWS are rather weak and partially blended together so that the resolution of the LWS (150 at 44 μm) is not sufficient to determine their strength with sufficient accuracy. Hence one has to rely on extrapolations for a comparison between the two spectrometers – a somewhat problematic method given the fact that there might be a feature of calcite present at 43.5 μm. Even though the difference between SWS and LWS is small, it might point towards a systematic discrepancy. It should be noted here that the only water lines which were observed with the LWS-FP (at 63 μm) gave an emissivity of 0.92, closer to the SWS value.

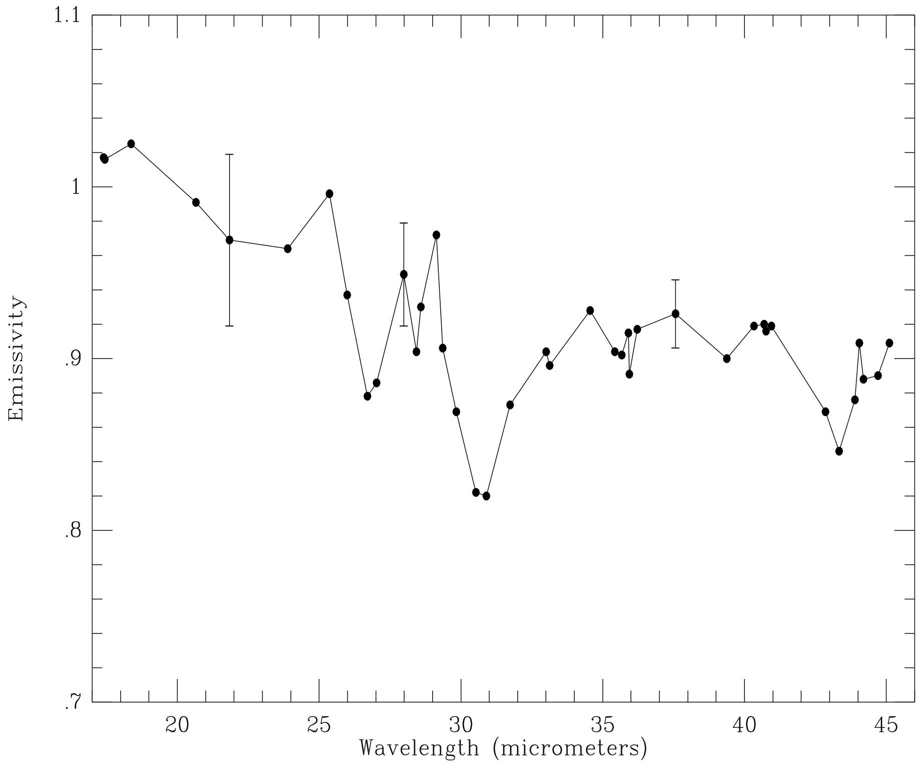

Figure 3.1: *Emissivity spectrum at 17 - 45 micron (Lellouch et al. 2000)*

3.1.2 Ammonia Lines on Jupiter

Several ammonia features were detected with high signal-to-noise ratio on Jupiter, both with SWS and with LWS. They can be very well fitted by the same model (see figures 11 and 12), hence showing that the line strengths obtained with the two spectrometers are compatible with one another.

3.1.3 HD and Water Lines on the Giant Planets

Water has been detected in the stratosphere of all Giant Planets with the SWS (Feuchtgruber *et al.* 1999). The line strengths found for the LWS-FP for the same molecule on Jupiter agree with the findings from the SWS.
For HD on Jupiter the same value was found from the R(2) line in the SWS range as from the R(0) line observed with the LWS.
Therefore one obtains the same abundances from SWS and LWS for all molecules on Jupiter which could be observed with both spectrometers.

3.2 Comparison between ISO and KAO Line Fluxes

This work has been performed by Leticia Martin on the following compact HII regions:

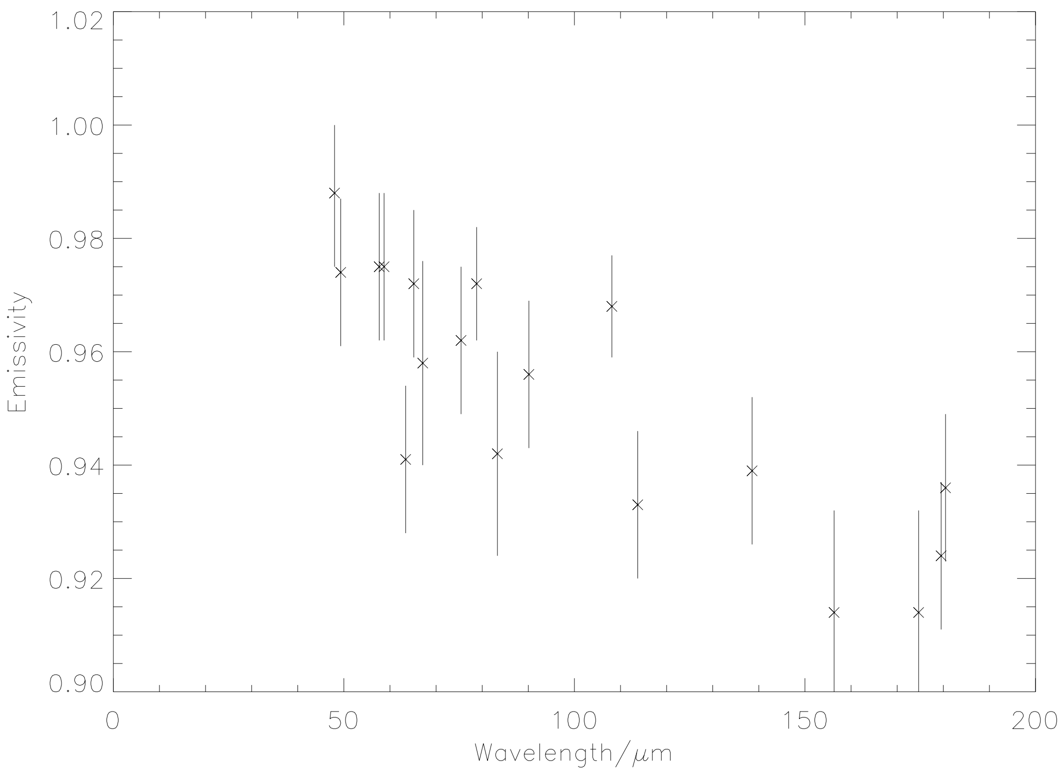

Figure 3.2: *Emissivity as a function of wavelength derived from line-to-continuum ratios in an LWS end-to-end grating scan. The error bars were derived from the line fit; there is an additional, systematic uncertainty of 0.02 due to the error margins in the water profile.*

Her findings are summarized in figure 13. The three lines analysed, at 52, 57 and 88 μm, give the same result at all fluxes: a slightly higher LWS than KAO line flux. This difference is less than 30 %.

3.3 Comparison between ISO and FILM Line Fluxes

There has been a dedicated observing program with LWS to map the CII line at 158 μm in a region that was also observed by the FILM (Far-Infrared Line Mapper) spectrometer aboard IRTS (Infrared Telescope in Space). The results from the two satellites are contradictory: The flux measured with FILM is only half the one of ISO. Similarly with BICE (Balloon-borne Infrared Carbon Explorer) only 60 % of the flux with ISO was found. It must be said, however, that BICE shows systematically smaller ($\approx$ 65 %) fluxes then COBE/FIRAS (Cosmic Background Explorer / Far-Infrared Absolute Spectrophotometer) observations (Nakagawa *et al.* 1998).

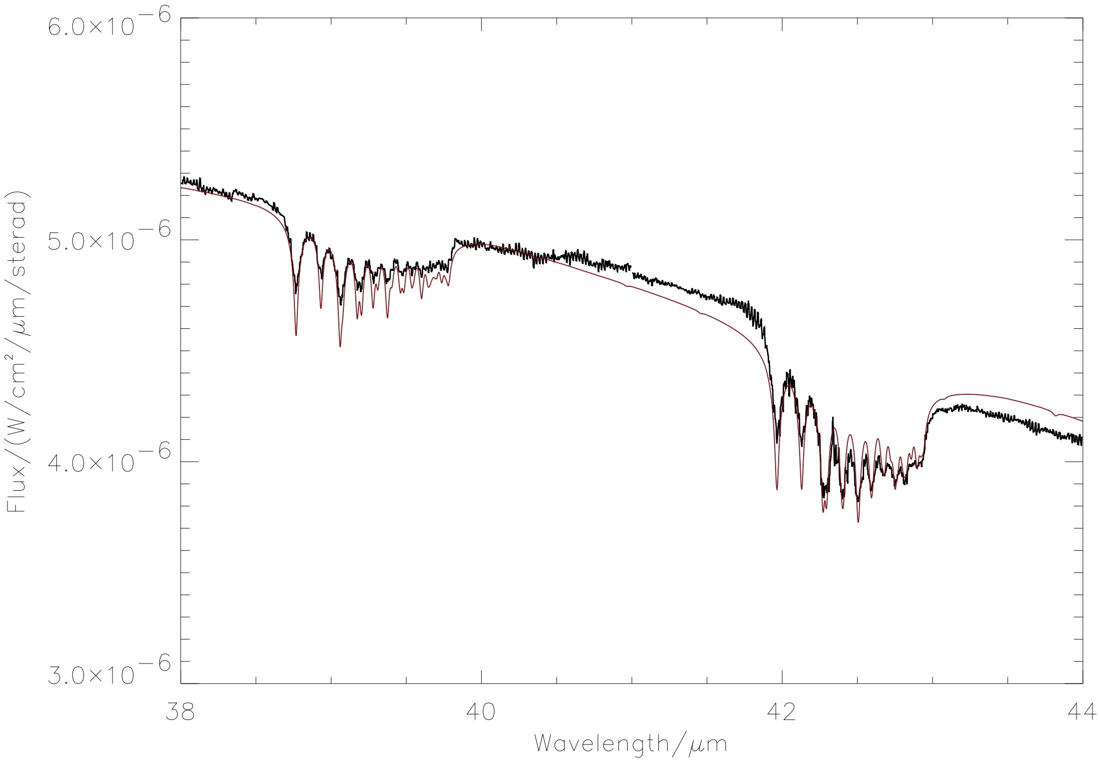

Figure 3.3: *Jupiter's spectrum between 38 and 44 micron. The measurement with the SWS is plotted in black, the model spectrum in red.*

Table 3.1: *HII Regions Used for Comparison LWS/KAO*

Source name	TDT number	KAO references
IRAS12073	25901573	Simpson 95
IRAS17455	28701328	Megeath 90, Simpson 95
IRAS17591	51500579	Afflerbach 97
IRAS18032	51500477	Afflerbach 97
IRAS18317	47801041	Simpson 95
IRAS18434	15201381	Herter 81, Megeath 90, Simpson 95
IRAS18479	15201792	Afflerbach 97
IRAS19110	49900901	Herter 81
IRAS19598	14601348	Megeath 90, Colgan 91
IRAS21270	82100310	Rudolph 97
IRAS21306	82301011	Rudolph 97
IRAS23030	22000962	Herter 82, Simpson 95

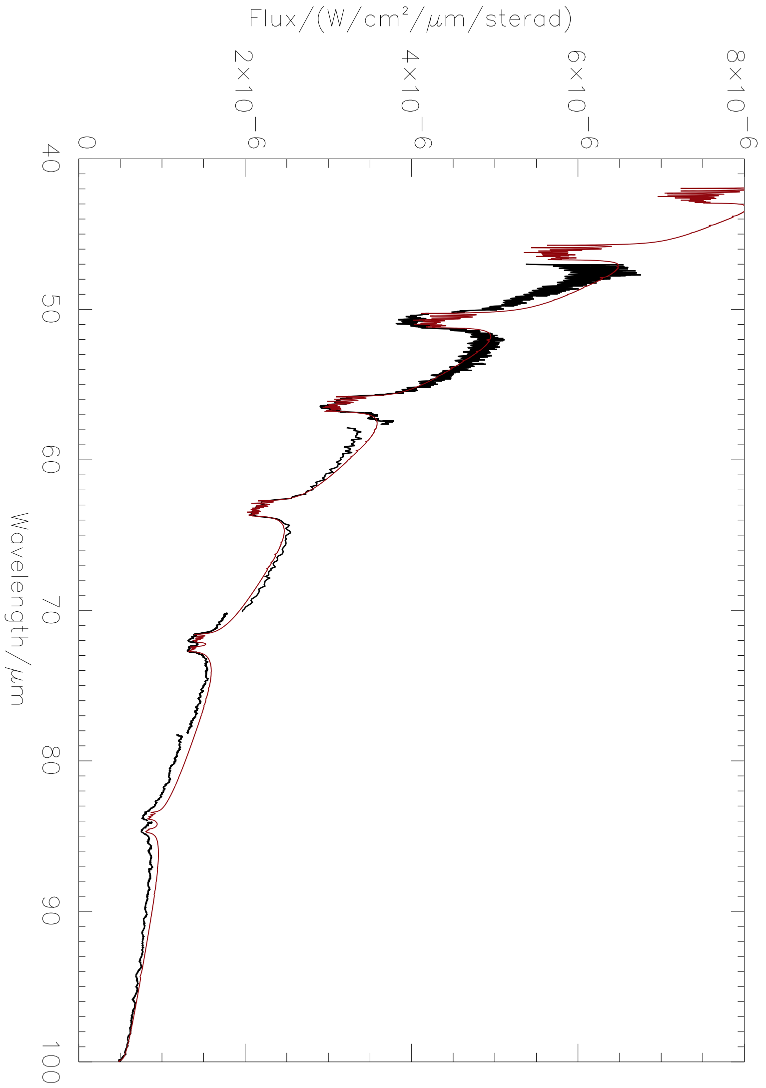

Figure 3.4: *Jupiter's spectrum between 47 and 100 micron. The measurement with the LWS is plotted in black, the model spectrum in red (Burgdorf et al. 2001).*

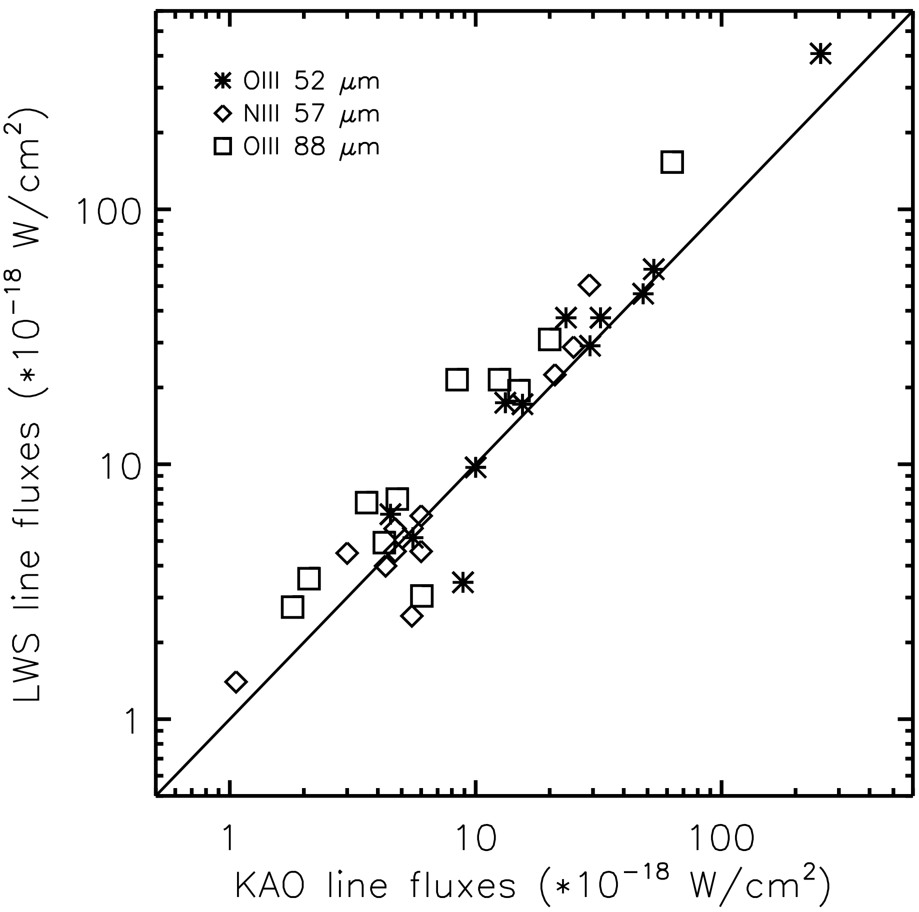

Figure 3.5: *Comparison of the forbidden lines in both LWS and KAO for compact HII regions (Peeters, Martin et al.)*

Chapter 4

Comparison of Models for Solar System Objects

Solar System Objects are the only sources suitable for calibrating the far-infrared flux range above 100 Jy. They have the advantage of being point-like and their spectra are easy to model (Orton & Burgdorf 2001). We discuss in the following subsections for several examples of these objects how well SWS and LWS agree with each other and with model spectra.

4.1 Mars

For two reasons it is important to check the agreement between the spectrometers aboard ISO on Mars:

- Mars is a widely used calibration standard in the far infrared
- the flux from Mars is one to two orders of magnitudes higher than that of other Solar System Objects with well known spectra

For these reasons it is possible to explore with Mars the validity of the flux calibration close to the upper limit of the dynamic range of the instruments. Several effects can cause non-linearities there. The signal can be so strong, as is the case for example in grating scans on Jupiter, that it is outside the range with which the electronics can cope. For somewhat weaker sources, like Saturn, "debiasing" occurs, a well known problem with integrating amplifiers (Leeks *et al.* 2001). As the photocurrent of the detector charges the input capacitance of its amplifier, the potential on this side of the detector increases. As a result the effective bias across the detector decreases with the consequence of a decreasing responsivity. But even in the absence of saturation and debiasing effects the detector responsivity might depend on the source flux; this phenomenon has been studied carefully by the PHT team (see

`http://www.iso.vilspa.esa.es/users/expl_lib/PHT_list.html`

). Figures 14 and 15 show the flux of Mars measured directly (i. e. not via the water lines, see chapter 2.2.1) with the two spectrometers aboard ISO. The agreement is about 10 %; this is remarkably good given the fact that the LWS spectrum is not corrected for debiasing. It must be said, however, that the LWS detector SW1, i. e. the one at the short wavelength end, was completely off-scale and therefore was excluded from this study.
The measured spectrum of Mars agrees well with a model for the Martian continuum by Don Rudy (Rudy *et al.* 1987).

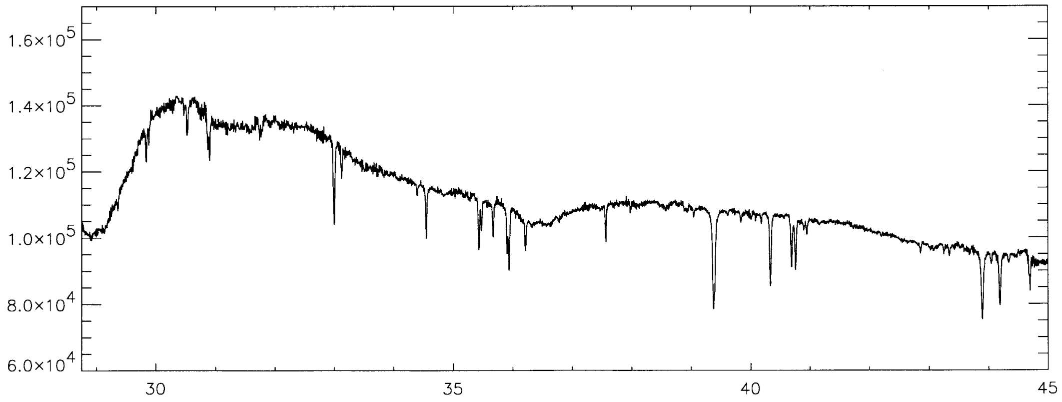

Figure 4.1: *The spectrum of Mars in band 4 of the SWS*

4.2 Ceres and Callisto

Observations of the Galilean satellite Callisto have provided far infrared calibration information for both SWS and LWS in the upper flux regime ($\approx$ 1000–2000 Jy). The maximum elongation from Jupiter of 10' is sufficient to exclude distortions originating from the bright Jupiter disk up to wavelengths of $\approx 100\ \mu$m. The mismatch between SWS and LWS on Callisto (see figure 16) was the first case of that kind which was investigated in the Spectral Matching Working Group. It can be seen from the comparison with a model originally developed to derive thermal properties of asteroids (Müller & Lagerros 1998) that only band 4 of the SWS and, to a lesser extent, detector SW1 of the LWS, are problematic. Hence matching the model to the spectrum measured at shorter and longer wavelengths, where the instruments are well behaved, can serve to determine a correction function to be applied to band 4 and SW1.

4.3 Uranus and Neptune

Two grating spectra over large wavelength ranges were recorded with the SWS on Neptune in October 1996. For the comparison with the LWS, we analysed only the wavelength range $29 - 45\ \mu$m. In this region of the spectrum H_2 - H_2 and H_2 - He collision-induced absorption features can be found which provide constraints to the models of the atmosphere and therefore allow an indirect comparison with the LWS range. At shorter wavelengths the flux from Neptune is too weak to achieve a reasonable signal-to-noise ratio. The typical errors in the absolute photometric calibration for band 4 of the SWS can amount up to 35 % (Salama *et al.* 1997), so every agreement with LWS that lies within this range must be considered satisfactory.

The spectrum of Neptune between 45 and 196 μm was measured with the LWS. We used 14 observations in photometric mode, i. e. doing narrow-band photometry with the grating in fixed position (AOT L02), to obtain highly accurate fluxes at ten points in the LWS wavelength range. These were complemented by 15 observations of the same kind on Uranus which served as reference measurements on which the calibration was based.

The results are shown in figure 17. It provides also a comparison with the Voyager IRIS results

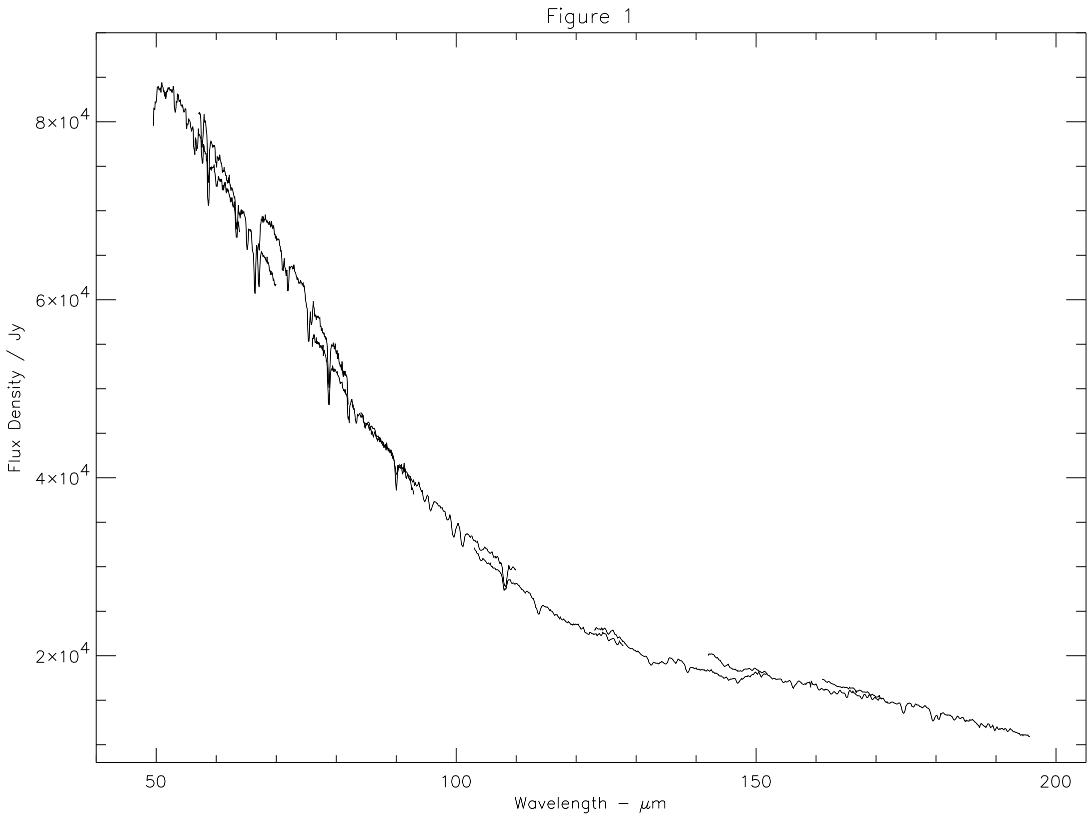

Figure 4.2: *A typical scan-averaged spectrum of Mars in the LWS wavelength range, showing an abundance of water vapour lines. (Sidher et al. 1998)*

and shows a remarkably good agreement between all data sets and Glenn Orton's model. Therefore we suggest to use in the future this model of Neptune's spectrum as a reference, together with Uranus, for the photometric calibration in the far infrared, when stars are not suitable.

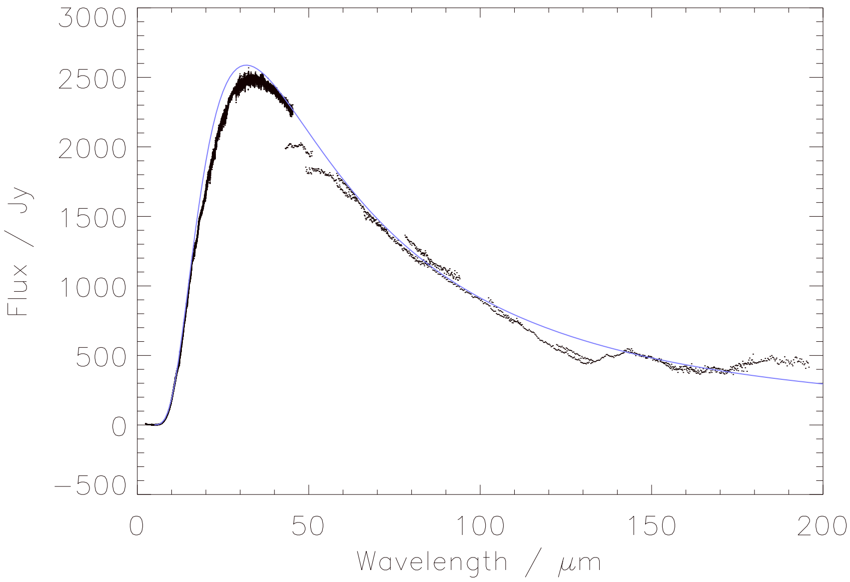

Figure 4.3: *End-to-end Spectrum of Callisto compared to a model*

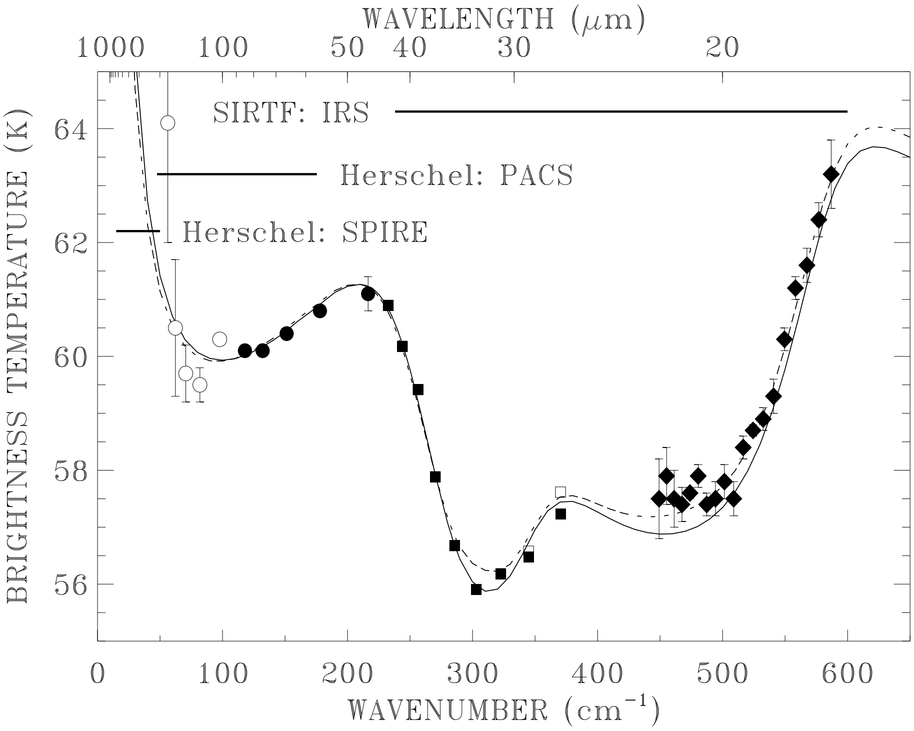

Figure 4.4: *Brightness temperature spectra of Neptune's disk, showing a schematic representation of the spectral ranges of the SIRTF (Space Infrared Telescope Facility) Infrared Spectrometer (IRS), and the planned FIRST (Far Infrared Telescope Facility) Photoconductor Array Camera and Spectrometer (PACS) and Spectral and Photometric Imaging REceiver (SPIRE) instruments. Model spectrum in the solid line is the best fit to the ISO data alone, and in the dashed line to the combination of ISO and ground-based data.*

Chapter 5

Conclusions and Relevance for Future Space/Airborne Observatories

ISO is the only observatory that could take end-to-end spectra from 2 to 200 μm. Even though these spectra consist of many different bands and were taken with many different detectors, they match very well. Therefore they can be used to improve existing calibration standards. With ISO it was possible to measure for the first time with high accuracy the emissivity of Mars in the far infrared. In addition to that we got accurate 2 - 200 μm spectra for Ceres and Callisto, the spectrum of Uranus was checked against Mars, and Neptune was established as far-infrared standard. Hence we have now a much larger selection of continuum sources with well-known spectra than five years ago, and this is an obvious legacy of ISO for the calibration of future missions.

Arriving at this conclusion took a lot of work by the Instrument Dedicated Teams in VilSpa and the PI teams at the home institutes. This cooperation proved to be very successful in calibrating the spectrometers aboard ISO. The report presented here shows that also collaboration across the borders of the different instruments is necessary to obtain a homogeneous dataset from all ISO observations. It is recommended for future missions to provide coordination between the different instruments, e. g. in the question which model to use for a common calibration standard, already during the operational phase.

Bibliography

[1] Afflerbach, A., Churchwell, E., Werner, M.W. 1997, Galactic Abundance Gradients from Infrared Fine-Structure Lines in Compact H II Regions, *Astrophysical Journal*, **478**, 190–205

[2] Brauher, J., Lord, S. 2001, The ISOLWS-IRAS Cross-Calibration of Extragalactic Sources, *ESA SP-481*

[3] Brock, D., Joy, M., Lester, D.F., Harvey, P.M., Ellis, H.B. 1988, Far-infrared observations of a luminous dust-shrouded source in the nucleus of NGC 4945, *Astrophysical Journal*, **329**, 208–211

[4] Burgdorf, M.J., Encrenaz, T., Lellouch, E., Feuchtgruber, H., Davis, G.R., Swinyard, B.M., de Graauw, T., Morris, P.W., Sidher, S.D., Griffin, M.J., Forget, F., Lim, T.L. 2000, ISO Observations of Mars: An Estimate of the Water Vapor Vertical Distribution and the Surface Emissivity, *Icarus*, **145**, 79–90

[5] Burgdorf, M., Feuchtgruber, H., García-Lario, P., Müller, T., Salama, A., Lord, S., Lahuis, F., Martn, L. 2001, Matching the Spectrometers on board ISO, *ESA SP-481*

[6] Colgan, Sean W.J., Simpson, J.P., Rubin, R.H., Erickson, E.F., Haas, M.R., Wolf, J. 1991, Far-infrared lines from G45.13 + 0.14 A and K3-50 A – Density fluctuations in compact H II regions, *Astrophysical Journal*, **366**, 172–180

[7] Feuchtgruber, H., Lellouch, E., Encrenaz, T., Bezard, B., Coustenis, A., Drossart, P., Salama, A., de Graauw, T., Davis, G.R. 1999, Oxygen in the stratospheres of the giant planets and Titan, *ESA SP-427*, 133–136

[8] Ghosh, S.K., Bisht, R.S., Iyengar, K.V.K., Rengarajan, T.N., Tandon, S.N., Verma, R.P. 1992, Far-infrared observations of NGC 4945 and the Circinus galaxy, *Astrophysical Journal*, **391**, 111–120

[9] Herter, T., Helfer, H.L., Briotta, D.A., Forrest, W.J., Houck, J.R., Rudy, R.J., Willner, S.P., Pipher, J.L. 1982, Abundances in five nearby galactic H II regions from infrared forbidden lines, *Astrophysical Journal*, **262**, 153–163

[10] Herter, T., Helfer, H.L., Forrest, W.J., McCarthy, J., Houck, J.R., Willner, S.P., Puetter, R.C., Rudy, R.J., Soifer, B.T., Pipher, J.L. 1981, Abundances of argon, sulfur, and neon in six galactic H II regions from infrared forbidden lines, *Astrophysical Journal*, **250**, 186–199

[11] Megeath, S.T., Herter, T., Gull, G.E., Houck, J.R. 1990, Infrared and radio measurements of the density structure of compact H II regions, *Astrophysical Journal*, **356**, 534–543

[12] Leeks, S.J., Swinyard, B.M., Clegg, P.E. 2001, The Correction for LWS Detector De-biasing of Strong Source Data, *EAS SP-481*

[13] Lellouch, E., Encrenaz, T., de Graauw, T., Erard, S., Morris, P., Crovisier, J., Feuchtgruber, H., Girard, T., Burgdorf, M. 2000, The 2.4–45 μm spectrum of Mars observed with the infrared space observatory, *Planetary and Space Science*, **48**, 1393–1405

[14] Müller, T.G., Lagerros, J.S.V. 1998, Asteroids as far-infrared photometric standards for ISOPHOT, *Astronomy and Astrophysics*, **338**, 340–352

[15] Nakagawa, T., Yui, Y.Y., Doi, Y., Okuda, H., Shibai, H., Mochizuki, K. 1998, Far-Infrared [C II] Line Survey Observations of the Galactic Plane, *Astrophysical Journal Supplement Series*, **115**, 259–269

[16] Orton, G., Burgdorf, M. 2001, Planetary Spectral Models as References for Calibration, *EAS SP-481* bibitem Rubin, R.H., Simpson, J.P., Erickson, E.F., Haas, M. R. 1988, Determination of N/O from far-infrared line observations of Galactic H II regions, *Astrophysical Journal*, **327**, 377–388

[17] Rudolph, A.L., Simpson, J.P., Haas, M.R., Erickson, E.F., Fich, M. 1997, Far-Infrared Abundance Measurements in the Outer Galaxy, *Astrophysical Journal*, **489**, 94–101

[18] Rudy, D.J., Muhleman, D.O., Berge, G.L., Jakosky, B.M., Christensen, P.R. 1987, Mars – VLA observations of the northern hemisphere and the north polar region at wavelengths of 2 and 6 cm, *Icarus*, **71**, 159–177

[19] Salama, A., Feuchtgruber, H., Heras, A., Lahuis, F., Leech, K.J., Lorente, R., Morris, P., van den Bussche, B., Wieprecht, E. 1997, Topics in SWS Data Analysis and Calibrations, *ESA SP-419*, 17–22

[20] Sidher, S.D., Griffin, M.J., Davis, G.R., Swinyard, B.M., Burgdorf, M., Orton, G.S., Encrenaz, T., Lellouch, E., de Graauw, T. 1998, ISO LWS Observations of Mars – a Search for Rotational Variability, *ESA SP-427*, 189–192

[21] Sidher, S.D., Swinyard, B.M., Harwood, A.S., Lord, S.D., Unger, S.J. 1997, The LWS Interactive Analysis Software, *ESA SP-419*, 297–298

[22] Simpson, J.P., Colgan, S.W.J., Rubin, R.H., Erickson, E.F., Haas, M.R. 1995, Far-infrared lines from H II regions: Abundance variations in the galaxy, *Astrophysical Journal*, **444**, 721–738